Processing and Interpretation of Crack-Propagation Sensors

Nenad G. Nenadic[1], Paul A. Ardis[2], Adrian Hood[3], Michael G. Thurston[4], and David G. Lewicki[5]

[1,4] *Rochester Institute of Technology, Rochester, NY, 14526, USA*
nxnasp@rit.edu
mgtasp@rit.edu

[2] *GE Global Research Center, 1 Research Circle, Niskayuna, NY, 12309*
ardis.p@ge.com

[3] *US Army Research Laboratory, 4603 Flare Loop, Aberdeen Proving Ground, MD 21085*
adrian.a.hood.civ@mail.mil

[5] *NASA Glenn Research Center, 21000 Brookpark Rd. - MS 23-3, Cleveland, OH 44135*
david.g.lewicki@nasa.gov

ABSTRACT

The goal of gearbox prognostics, once a failure has been detected, is to estimate the degree of damage. Development of probabilistic damage assessment requires high quality ground truth. The present report describes practical analysis, processing, and interpretation of signals from crack-propagation sensors and damage estimation during gear teeth crack propagation. The study considers two types of crack propagations: one for a fatigue-tester-based crack propagation, and the other for a propagation in a gearbox. Crack closing occurs in both types of crack propagation and must be accounted for in assessing the damage. The analysis is conducted for sensors connected as a voltage divider. Signal conditioning and wire breakage inference are examined in detail. In addition, we discuss how equipping each gear tooth with two crack-propagation sensors, one on each gear face, can provide a better damage estimation.

1. INTRODUCTION

Of the four dominant modes of gear tooth failure (breakage, wear, pitting, and scoring), breakage is the most catastrophic and occurs precipitously, often with no advanced warning. From the fatigue viewpoint a life time of a gear can has two phases: crack initiation and crack propagation (Kramberger, Šraml, Potrč, & Flašker, 2004; Kramberger, Šraml, Glodež, Flašker, & Potrč, 2004; Glodež, Šraml, & Kramberger, 2002). Gear research community has developed many vibration-based, condition indicators (CIs), to detect these features and assess damage, as summarized in (Lebold, McClintic, Campbell, Byington, & Maynard, 2000; Samuel & Pines, 2005). To validate the performance of these CIs, researchers has been employing crack propagation (CP) sensors (see e.g. (Zakrajsek & Lewicki, 1998; N. Nenadic et al., 2013)). The physical principle of CP sensors is the change in resistance as a function of crack length. These sensors consist of thin, parallel strands of known resistance which snap as the crack propagate through and the total resistance increases.

Crack propagation sensors are typically used to measure crack lengths on the surface of mechanical structures. This study is focused on the analysis of signals from CP sensors implemented on spur gears. Two types of tests are considered: crack propagation in a single-tooth fatigue-based tester and crack propagation inside a gearbox. The initial cracks were not notched but imparted using fatigue overload (N. G. Nenadic, Wodenscheck, Thurston, & Lewicki, 2011; Stringer, LaBerge, Burdick, & Fields, 2012). In both cases the CP sensors provide measurable ground truth for the level of damage.

After the signals are conditioned and interpreted, they can be used to assess the damage on the face and predict the internal crack. In the first approximation the damage is expressed as the *crack length*. For a conservative approach, the selected length would be the longer of the two crack lengths, visible on the faces of the gear. However, the cracks often do not propagate uniformly across the face of a gear tooth. Lewicki et al. (Lewicki, Sane, Drago, & Wawrzynek, 1998) studied crack surfaces computationally, using boundary element methods. The information of crack lengths on both gear faces can be used to estimate these wavefronts and, more generally, to es-

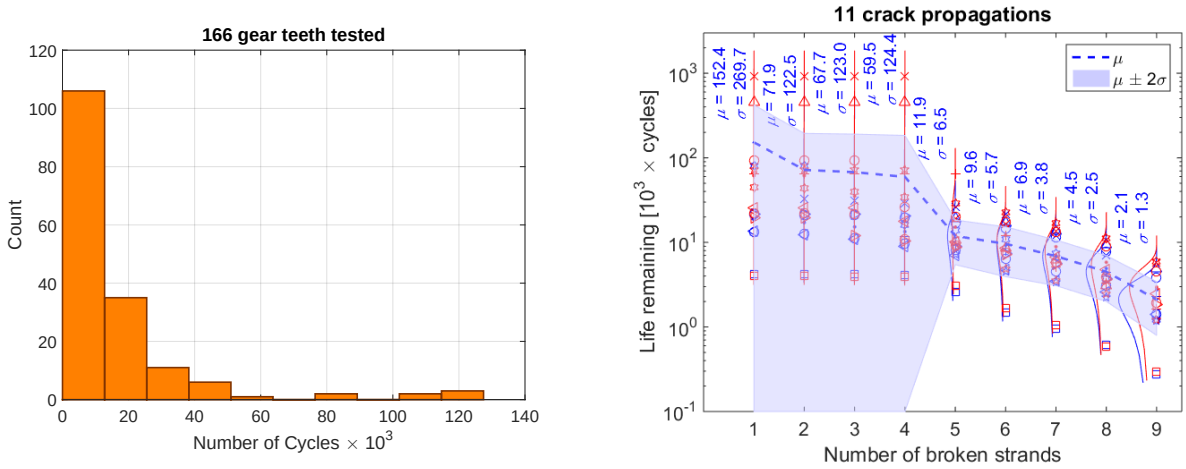

(a) (b)

Figure 1. (a) Histogram of cycles needed to initiate the cracks (b)Life remaining in cycles distributions vs. the crack size as measured on gear faces with crack-propagation sensors.

timate the overall crack damage.

The importance of damage estimation becomes immediately clear when considering a large number of individual crack propagations. Because crack propagation on a fatigue tester is a less expensive and less complex experiment than a crack propagation in a gearbox, a statistically large collection of cracks was obtained on the single-tooth, fatigue tester. Figure 1a shows a histogram of the of cycles to induce a crack under fixed conditions for 166 gear teeth. Fatigue cracks were initiated on 93% of gear teeth before 50,000 cycles and 85% before 30,000 cycles. With an excitation frequency of 5 Hz, 85% of cracks were initiated within 100 minutes.

While the large uncertainty in crack initiation is to be expected, crack propagation is considered much better understood. For example, Paris Law (Paris, Gomez, & Anderson, 1961) has a long history of successful practical use; it is given by

$$\frac{da}{dN} = C(\Delta K(a))^m, \tag{1}$$

where a is the crack size, N is the number of cycles, and m, C, and $K(a)$ are material properties. However, the experiments show that evolution of small cracks can also have considerable uncertainty, especially initially, when fatigue-induced cracks are small and asymmetric.

After crack initiation, the tooth was subjected to a cycling excitation until the crack propagated until all the strands on both crack propagation sensors were broken. Figure 1b shows the remaining useful life (RUL) vs damage size for 11 of the 166 tested gear teeth, with the statistical information superimposed. Individual propagations are indicated by markers, with normal distributions estimated for each number of broken strands. Two different colors signify the crack lengths on two different sides of a gear. Note the square markers at the bottom: they denote a propagation where the crack lengths were about equal on both faces. In our experiments, these *symmetric* cracks propagate considerably faster than their *asymmetric* counterparts. The shaded area signifies two standard deviations about the mean. For small cracks (low number of broken strands), the life remaining is not normally distributed and the uncertainty is very large (note that the y-axis scale is logarithmic). After the 4th strand broke (which is corresponds to crack length of about 1.3 mm), the propagation accelerated for most of the gear teeth. Thus, crack length of 1.3 mm denotes prognostics horizon and in this region, Paris' Law given by Eq. (1) can be reasonably fitted. Note, however, that for this gear and this loading, there is only 12,000 cycles left after the horizon is reach. An angular speed is needed to translate the prognostic horizon in time. For example, for an angular speed at ω = 1200 rpm = 20 rad/s, the prognostic horizon is only 600 seconds, or 10 minutes.

2. SENSOR PLACEMENT AND SENSING CIRCUIT

While our results are quite general, further elements of the particular implementation are described in detail. This section provides specific aspects of sensing during the test of this study. Each sensor is placed so that it strands are approximately perpendicular to a typical path of crack propagation (Lewicki et al., 1998). We designed a mask, shown in Figure 2, to ensure close agreement in sensor placements among samples.

Figure 3 shows the circuit diagram for the CP sensor, based on Kelvin (four-wire) connection, where R_s is the pull-up source resistor, V_{ss} is the power supply voltage, R_{cp} signifies the resistance of the crack-propagation sensor, and I is the current. Four-wire measurement method is employed to minimize the effect of the lead wires indicated by R_W in Fig-

Figure 2. Design mask overlaid on top of a gear.

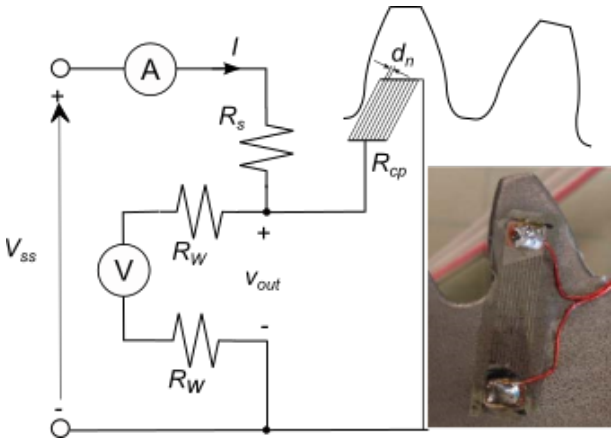

Figure 3. The circuit diagram for 4-wire connection of a CP sensor. The inset shows an image of a real, instrumented tooth.

ure 3. Voltage drop across lead resistance R_W can be important when measuring small resistances. Two additional, sensing leads create a high-impedance loop, which minimizes the current the current through R_W and thus minimize the voltage drop across R_W; see e.g., (Yeager & Keithley, 1998) for more details on four-wire connection and low (resistance) level measurements..

The output voltage v_{out} is the voltage divider across the CP sensor, given by

$$v_{out} = \frac{R_{cp}}{R_{cp} + R_s} V_{ss} \tag{2}$$

The resistance of individual strand R_{is} is 50 Ω. The total resistance of the CP sensor with k unbroken strands is $R_{cp} = R_{is}/k$ and the output voltage v_{out} is

$$v_{out} = \frac{R_{is}}{R_{is} + kR_s} V_{ss} \tag{3}$$

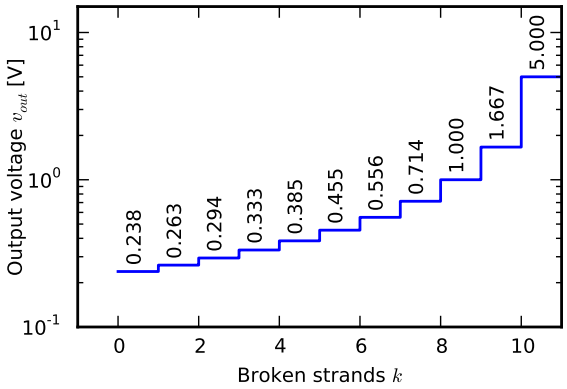

Figure 4. Computed voltage levels of the CP sensor for R_s = 100 Ω and V_{ss} = 5 V.

Table 1. Theoretical voltage levels for three different values of the pull-up resistor R_s and supply voltage V_{ss} = 5 V.

Broken wires k	v_{out} [mV] (R_s = 100 kΩ)	v_{out} [mV] (R_s = 1 kΩ)	v_{out} [mV] (R_s = 100 Ω)
0	0.25	24.9	238.10
1	0.28	27.6	263.16
2	0.31	31.1	294.12
3	0.36	35.5	333.33
4	0.42	41.3	384.62
5	0.50	49.5	454.55
6	0.62	61.7	55.56
7	0.83	82.0	714.29
8	1.25	122.0	1000.00
9	2.50	238.1	1666.67
10	5000.00	5.000	5000.00

The manufacturer of CP sensors does not recommend their utilization with pull-up resistor R_s smaller than 100 kΩ to limit the current through the CP sensor. However, to increase the sensitivity we reduced the value of the pull-up resistor down to R_s = 100 Ω. We have not observed any damage to the sensor during our testing. Figure 4 shows the output voltage v_{out} as a function of the number of the broken strands for the supply voltage V_{ss} = 5 V. The voltage level for each state of the CP sensor are indicated in the plot. Table 1 shows the computed voltage levels for three different pull-up resistors (recommended 100 kΩ, and employed 1 kΩ /100 Ω).

3. INTERPRETATION OF CP SIGNALS IN SINGLE-TOOTH CRACK PROPAGATION

The first type of tests propagated a crack on a single-tooth test fixture. After the crack is initiated on a single tooth and verified using magnetic particle inspection (N. G. Nenadic et al., 2011), the crack is propagated by applying a sinusoidal load with an offset $F(t) = F_o + F_{max} \sin(2\pi ft)$, with F_o = 750 lb (3,336 N), F_{max} = 650 lb (2,891 N), and f = 20 Hz (see the right axes of the inset of Figure 6). The drawing

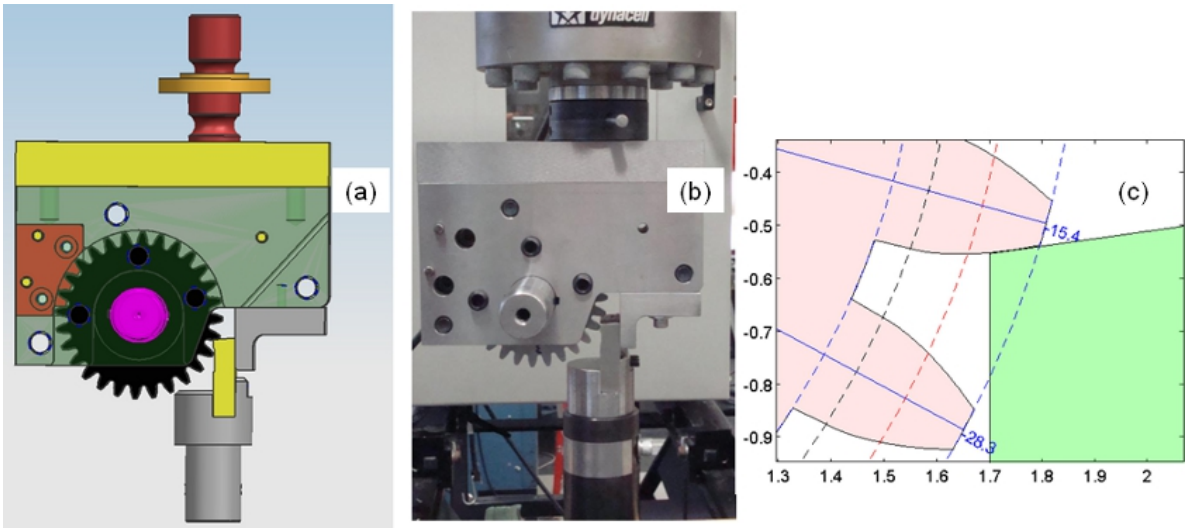

Figure 5. Single-tooth crack-initiation and crack-propagation fixture. (a) Drawing. (b) Photograph. (c) Sketch depicting point of contact.

of the fixture is shown in Figure 5a. The anvil pushes a single tooth at the prescribed load, while the reaction is shared among three reaction teeth. The photograph of the assembled fixture is shown in Figure 5b. The anvil applies the force at the highest point of single tooth contact (HPSTC). Figure 5c shows a close-up diagram of the contact between the tooth under test and anvil.

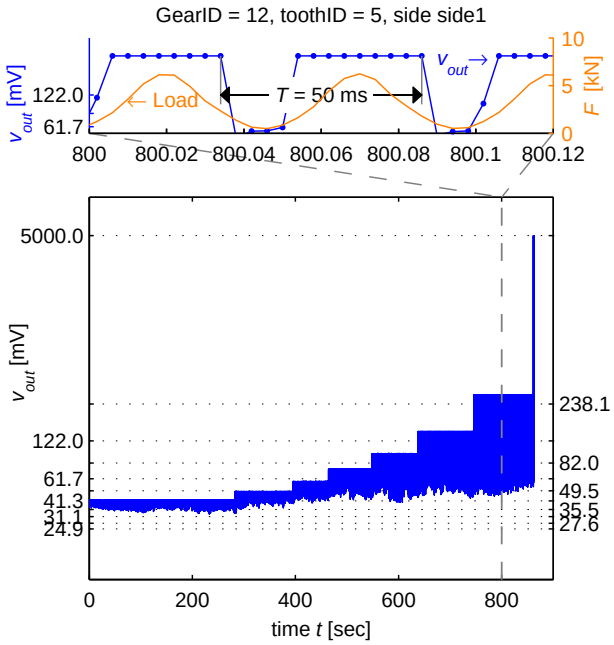

Figure 6. Raw data captured on the single-tooth for R_s = 1 kΩr and V_{ss} = 5 V.

Figure 6 shows an example raw voltage signal obtained from a CP sensor during a test on the single-tooth tester. The information of the crack propagation is contained in the envelope of the signal. The raw signal is not strictly non-decreasing because of the crack closing. The effect of crack closing is further illustrated in the inset of Figure 6, which shows the voltage signal over much shorter time scale. The waveform of the force applied via the anvil is overlaid (with the scale provided on the right-hand side). The step levels of the envelope of the measured signal do not perfectly line up with the computed levels, indicated by the grid lines. The imperfect match between measured and computed levels is hypothesized as due to the resistance of individual wires of the CP sensor are not precisely 50 Ω.

An example of a processed data is shown in Figure 7. The blue traces correspond to the left y-axis and indicate the processed crack propagation voltage; the solid trace corresponding to one of the crack-propagation sensors, denoted as *front*, and the other to the other sensor, denoted as *back*. The red traces correspond the right y-axis and indicate the length of the crack estimated based on the number of broken strands of the crack-propagation sensor in inches. The estimated length of the crack is simply as the normal distance between the strands d_n (see Figure 3) of a CP sensor multiplied by the number of broken strands k: $\hat{l} = kd_n$. The normal distance between the strands is $d_n = 0.01'' = 0.254$ mm. For simplicity, the plot assumes linear growth between cycles.

4. INTERPRETATION OF CP SIGNALS IN A GEARBOX

The second type of test propagated a gear tooth crack inside a gearbox loaded using dynamometer fixture. This proved to be a much electrically noisier environment due to a slip-ring requirement. The gear was rotated at ω = 1500 rpm producing a toothmesh period of $2\pi/(28\omega) \sim 9$ ms (a gear has 28

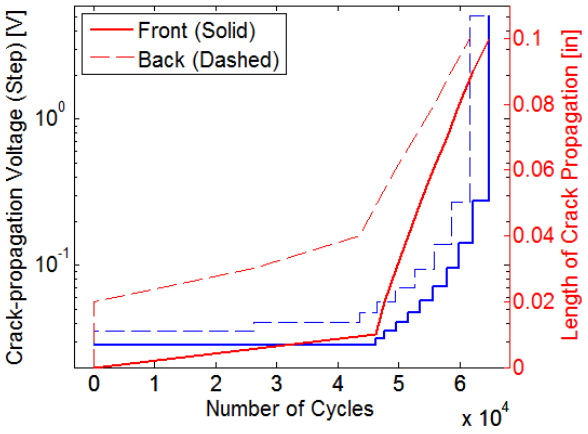

Figure 7. Processed cracks on tooth

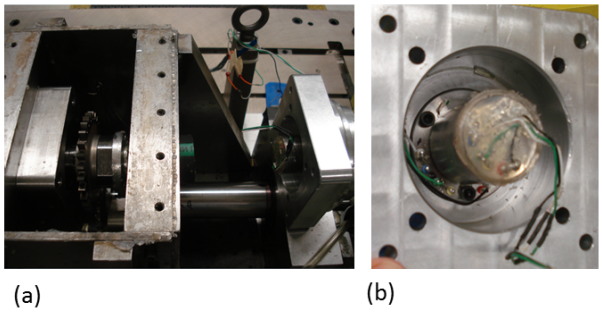

Figure 8. Gearbox fixture built on a dynamometer (a) open gearbox (b) slip ring

teeth). This tooth loading duration is a fraction of that experienced on the fatigue tester. Thus, the tooth loading duration is ∼4.5 ms. Relative duration of the applied load to the cracked tooth is much shorter 3.6% (100/28) of the cycle. In addition, to connect to the rotating instrumented gear teeth the signals are transmitted via slip-rings which add more noise to these feeble electrical signals. Figure 8a shows a part of a disassembled fixture with two gears meshed directly. Figure 8b shows the slip ring.

Figure 9 shows example waveforms midway through a propagation (compare the time line of Figure 9 to that of Figure 10). The subplot on top shows the waveform of the tachometer. The middle subplot shows a waveform of a less developed crack and the bottom shows the waveform of a more developed crack, where the effects of crack opening and closing can be readily observed.

Post-processing of the CP sensor signals was performed in order to remove noise artifacts prior to use as ground truth in detection and assessment tasks. As mentioned earlier, these artifacts took two forms: false "open" readings caused by intermittent slip ring failure, and voltage "jitter" caused by inconstant power supply. Correction for these artifacts was performed using global and local outlier rejection, respectively, as summarized in Algorithm 1.

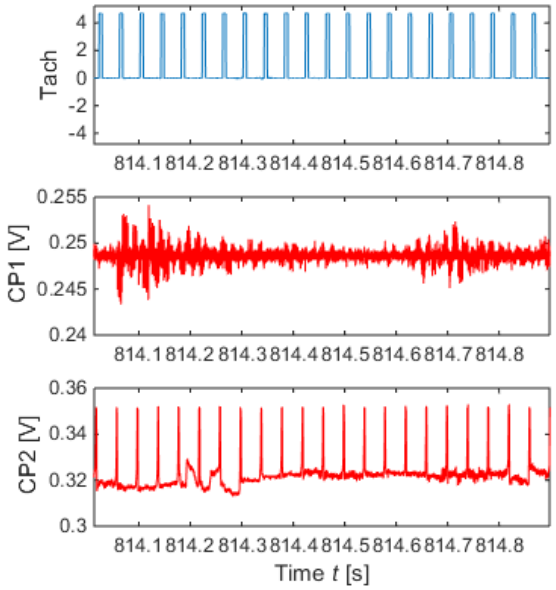

Figure 9. Raw CP data from a gearbox with a tach signal.

Algorithm 1 CP Postprocessing Algorithm

procedure POST-PROCESS(s, n, ϵ)
  // s is raw CP signal
  // n is length of signal
  // ϵ is Δ voltage threshold (%) for step detection
  Global(s, n)
  Local(s, Steps(s, n, ϵ))
end procedure

False openings are characterized by short, disconnected periods of approximately-full voltage observation, rapidly returning to baseline behavior at the current level of propagation. These observations arise from periods of slip ring decoupling, where the rotating brushes become disconnected by sudden impulses. In our experiments, these impulses were most likely to occur periodically in conjunction with particular tooth compression and release, although not all impulses strictly matched these mesh periods. In order to remove false openings, we performed outlier suppression at twice the standard deviation of the raw signal values, replacing spurious readings with the global mean, as written in Algorithm 2.

Once false openings are corrected, the remaining artifacts are modeled as the result of a multiplicative noise factor resulting from aperiodic variation in input power supply and an additive base factor resulting from regular systemic loss. Given our interest in using the CP sensor signals for discrete baseline classification of propagation (used in conjunction with accelerometer-based vibration features), we chose to ignore

Algorithm 2 Suppress Global Outliers

procedure GLOBAL(s, n)
  // s is raw CP signal
  // n is length of signal
  FIR($s, 0.0001$)
  for $i \leftarrow 1, n$ **do**
    if abs(mean(s) $- s[i]$) $\geq 2 *$ std(s) **then**
      $s[i] \leftarrow mean(s)$;
    end if
  end for
end procedure

the additive factor as it would not affect computational ability to distinguish between propagation levels. For the multiplicative factor, we hypothesized that it was well approximated by a Gaussian process with mean of 1 (zero impact) and magnitude no greater than the minimum factor between two adjacent propagation levels, confirmed empirically. In order to remove outliers that could lie within the output range of other propagation levels, we first identified all voltage changes in excess of this process, indicative of steps from one propagation level to another. This is shown in Algorithm 3, where we explicitly identify and lock in observable steps as new voltage baselines.

Algorithm 3 Identify Voltage Steps

procedure $m =$ STEPS(s, n, ϵ)
  // s is global-filtered CP signal
  // n is length of signal
  // ϵ is Δ voltage threshold (%) for step detection
  $c \leftarrow 1$
  $k \leftarrow 0$
  $i \leftarrow 1$
  while $i < n$ **do**
    while abs($s[c] - s[i]$)$/s[c] \leq \epsilon$ **do**
      $i \leftarrow i + 1$
    end while
    $k \leftarrow k + 1$
    $m[k] \leftarrow c$
    $c \leftarrow i$
  end while
end procedure

Once voltage steps were identified, we then identified and suppressed all local outliers that could result in level confusion (*i.e.*, those with multiplicative factors in excess of half of the minimum factor between adjacent propagation levels); suppression was done via mean replacement, as shown in Algorithm 4. The result of this process was a CP signal with minimized potential for label confusion when used in classification, allowing us to progress with further experiments in crack detection and assessment.

The final result of a damage extraction is shown in Figure 10.

Algorithm 4 Suppress Local Outliers

procedure LOCAL(s, m)
  // s is global-filtered CP signal
  // m is vector of voltage step indices
  $m[0] \leftarrow 1$
  for $i \leftarrow 1, k$ **do**
    for $j \leftarrow m[i-1], m[i]$ **do**
      if abs(mean($s[m[i-1] : m[i]]$) $- s[j]$) $\geq$ std($s[m[i-1]:m[i]]$) **then**
        $s[j] \leftarrow$ mean($s[m[i-1]:m[i]]$)
      end if
    end for
  end for
end procedure

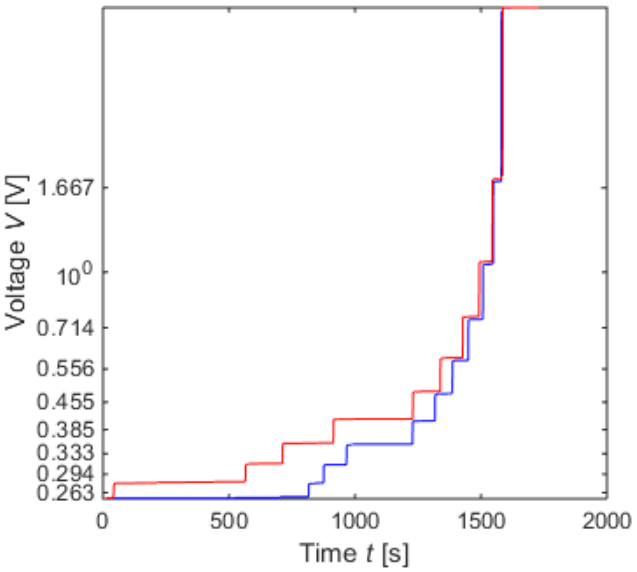

Figure 10. An example voltage levels parsed after a crack propagated in a gearbox
.

5. DAMAGE ESTIMATION AND FUTURE WORK

While cracks are typically thought of as lengths, in reality, they are surfaces. This quickly becomes apparent when one attempts to reconcile two different lengths, one on each gear face. Considerable information on damage and its likely future states may be contained in the relationship between the two lengths. For example, one can use breakage of CP strands to visualize a crack propagation, as illustrated in Figure 11. Here the data from CP sensors was used to plot two 3D stem plots (black traces), where the x-coordinates signify their physical location (the stem plots are separated by gear width w), y-coordinates signify propagation, expressed in terms of cycles N, and z-coordinates crack lengths (CP voltage levels mapped onto physical locations of particular strands and crack length estimated as the normal distance between strands). The blue traces indicate plausible wavefronts of the crack surface

propagation. These are not accurately estimated but can be nonetheless useful in assessing actual damage.

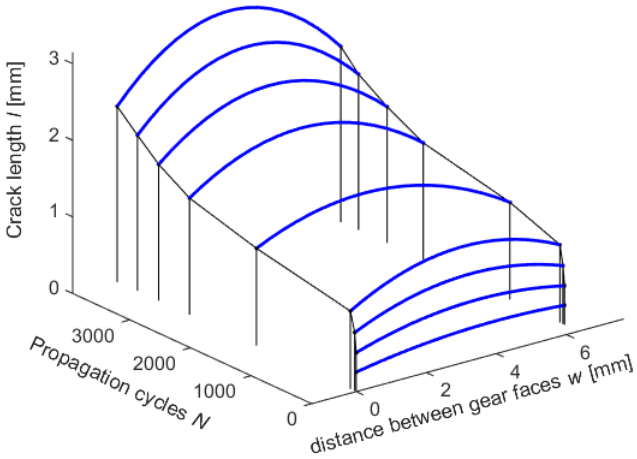

Figure 11. Estimated propagation wavefronts based on the CP data.

To obtain a better estimate of these damaged surfaces, it is necessary to perform a post-mortem analysis of the fractured surface. For example, Figure 12 shows a cracked surface of a gear tooth. Crack initiation phase, with larger forces and intergranular fracture, is readily distinguished from the crack propagation, with smaller forces and transgranular fracture (wavefront 1). Wavefronts 2-4 show different stages of crack propagation and wavefront 5 marks the boundary of the crack propagation and full fracture (in our experiments, propagation was stopped once the crack had propagated through both CPs and a large force was applied to fully fracture the tooth).

Future work will further investigate the opportunity of improving damage assessment of cracked teeth on spur gears by establishing correlations (in a broad sense) between the time-domain condition indicators extracted from non-destructive measurements and analysis of images of cracked surfaces during the post-mortem analysis. After applying material science expert knowledge to identify important damage features in the images, the correspondence between image features and temporal features will be sought. The ultimate objective is to enable damage assessment in the noisier, gearbox environments, which, in turn, would allow better damage assessment for diagnostic and prognostics, and thereby condition based maintenance.

6. CONCLUSIONS

Crack propagation sensors can provide valuable ground truth information on crack damage, which is essential for development of practical prognostics metrics. It may be important to capture the ground truth in more than one location because empirical results that show that crack lengths on two gear

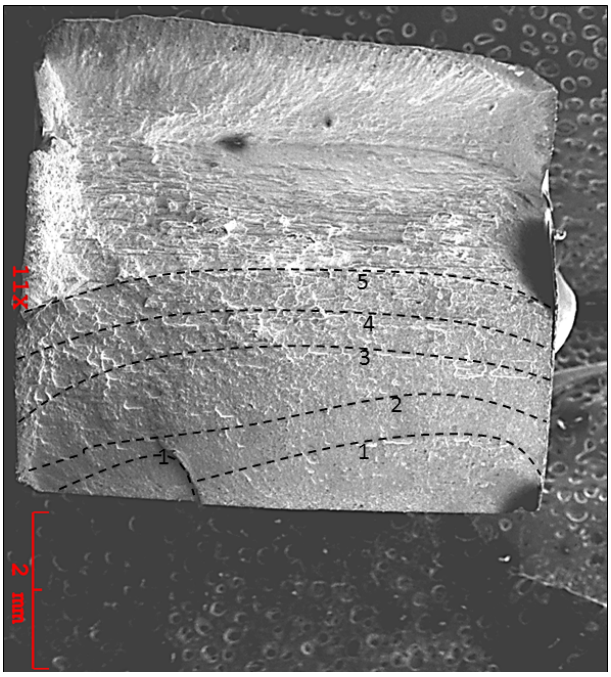

Figure 12. Cracked surface of a broken tooth with a few estimated wavefronts.

faces can differ considerably during a crack propagation and that the asymmetry may significantly affect the rate of the propagation. This paper describes extraction of this ground truth information on damage from noisy measurements. Two types of measurement settings were discussed: crack propagation on a fatigue tester and crack propagation in a gearbox. In both cases cracks close when the force is either removed or reduced. Information extraction from CPs is easier in the case of fatigue-tester propagation because gearbox instrumentation requires that slip rings, with their additional noise sources, be employed and because the relative opening of the crack in a gearbox is considerably shorter than the crack opening in the fatigue fixture. Finally, visualization of crack propagation, based on information from CPs is illustrated and the next steps of relating the temporal data and image features from the post-mortem analysis are

ACKNOWLEDGEMENTS

This work was made possible by the Office of Naval Research under Award No. N0004-07-1-0823 and Army Research Laboratory under Award No. W911NF-14-2-0029. The authors gratefully acknowledge the help of our colleagues from Rochester Institute of Technology: Joseph Wodenscheck and Art Dee for skilful LabVIEW implementation of the control for both fixtures; Joseph Wodenscheck, Allen Luccitti, Michael Bradly, and Robert Kosty for instrumenting gears with CP sensors, and Mark Walluk and Domenic Maiola for the mechanical design of the fixtures. This work would not have been possible without their contributions.

REFERENCES

Glodež, S., Šraml, M., & Kramberger, J. (2002). A computational model for determination of service life of gears. *International Journal of Fatigue*, *24*(10), 1013–1020.

Kramberger, J., Šraml, M., Glodež, S., Flašker, J., & Potrč, I. (2004). Computational model for the analysis of bending fatigue in gears. *Computers & structures*, *82*(23), 2261–2269.

Kramberger, J., Šraml, M., Potrč, I., & Flašker, J. (2004). Numerical calculation of bending fatigue life of thin-rim spur gears. *Engineering fracture mechanics*, *71*(4), 647–656.

Lebold, M., McClintic, K., Campbell, R., Byington, C., & Maynard, K. (2000). Review of vibration analysis methods for gearbox diagnostics and prognostics. In *Proceedings of the 54th Meeting of the Society for Machinery Failure Prevention Technology* (Vol. 634, p. 16).

Lewicki, D. G., Sane, A. D., Drago, R. J., & Wawrzynek, P. A. (1998). *Three-dimensional gear crack propagation studies* (Tech. Rep.). DTIC Document.

Nenadic, N., Ardis, P., Hood, A., Thurston, M., Ghoshal, A., & Lewicki, D. (2013). Comparative Study of Vibration Condition Indicators for Detecting Cracks in Spur Gears..

Nenadic, N. G., Wodenscheck, J. A., Thurston, M. G., & Lewicki, D. G. (2011). Seeding Cracks Using a Fatigue Tester for Accelerated Gear Tooth Breaking. In T. Proulx (Ed.), *Rotating Machinery, Structural Health Monitoring, Shock and Vibration* (Vol. 8, pp. 349–357).

Paris, P. C., Gomez, M. P., & Anderson, W. E. (1961). A rational analytic theory of fatigue. *The trend in engineering*, *13*(1), 9–14.

Samuel, P. D., & Pines, D. J. (2005). A review of vibration-based techniques for helicopter transmission diagnostics. *Journal of sound and vibration*, *282*(1), 475–508.

Stringer, D., LaBerge, K. E., Burdick, C. J., & Fields, B. A. (2012). *Natural Fatigue Crack Initiation and Detection in High Quality Spur Gears* (Tech. Rep.). DTIC Document.

Yeager, J., & Keithley, J. F. (1998). *Low level measurements: precision DC current, voltage and resistance measurements*. Keithley Instr.

Zakrajsek, J. J., & Lewicki, D. G. (1998). Detecting gear tooth fatigue cracks in advance of complete fracture. *Tribotest*, *4*(4), 407–422.

BIOGRAPHIES

Nenad Nenadic received his B.S. in Electrical Engineering from University of Novi Sad (Novi Sad, Serbia) in 1996 and his MS and Ph.D. in Electrical and Computer Engineering from University of Rochester (Rochester, NY, USA) in 1998 and 2001, respectively. He joined Kionix Inc. in 2001, where he worked on development of micro-electromechanical inertial sensors. Since 2005, he has been with Center for Integrated Manufacturing Studies (CIMS) at Rochester Institute of Technology, where he is currently a Research Associate Professor. His research interest include design, analysis, and monitoring of electromechanical devices and systems. He has two patents in electromechanical design and eight publications. He co-authored a textbook "Electromechanics and MEMS" and is a member of IEEE.

Paul Ardis received his B.S. in Computer Science and Mathematics from Purdue University (West Lafayette, IN, USA) in 2005 and his M.S. and Ph.D. in Computer Science from the University of Rochester (Rochester, NY, USA) in 2007 and 2009 respectively. He is Lead Scientist in the Machine Learning Lab at GE's Global Research Center, formerly Research Associate Professor at Rochester Institute of Technology and Research Scientist under contract to the Air Force Research Laboratory. He holds two patents in signal processing and has published thirteen scholarly articles in machine learning, computer and human vision, biometrics, and machine diagnostics and prognostics. His research interests include data-driven predictive modeling, decision theory, surveillance, natural language processing, and machine sensing..

Adrian Hood Adrian works in the Propulsion Division of the Army Research Lab's Vehicle Technology Directorate at Aberdeen Proving Ground, MD. His background is in helicopter transmission diagnostics. He earned his PhD in Aerospace Engineering at the University of Maryland, College Park.

Michael Thurston received his B.S. and M.S. in Mechanical Engineering from Rochester Institute of Technology (Rochester, NY, USA) in 1988, and his Ph.D. in Mechanical and Aerospace Engineering from the University of Buffalo (Buffalo, NY, USA) in 1998. He is the Technical Director and Research Associated Professor at the Center of Integrated Manufacturing Studies at Rochester Institute of Technology. He formerly held positions in air conditioning system development at General Motor and Delphi, and as a Researcher at the Applied Research Laboratory at Penn State University. He holds 7 patents in the areas of air conditioning and asset health monitoring. His research interests include: sustainable design and production, condition

based maintenance and prognostics, and asset health management. He is a member of the Society of Automotive Engineers, and was awarded the Boss Kettering Award for product innovation by Delphi.

David Lewicki is an employee of the NASA Glenn Research Center, Cleveland, Ohio, He started with NASA in August 2009. Prior to that, Dr. Lewicki was an employee of the U.S. Army Research Laboratory's Vehicle Technology Directorate at the NASA Glenn Research Center from 1982 to 2009. In his career, Dr. Lewicki has been performing analytical and experimental research in transmission, gearing, and bearing areas for rotorcraft and turboprop drive train applications. Specifically, he has been involved in research for the following areas: face gears for helicopter transmissions, low noise gears, gear crack propagation, gear diagnostics, engine disk crack detection, lubrication, transmission life and reliability predictions, gear dynamics, and variable-speed transmissions. Dr. Lewicki has earned a Ph.D. from Case Western Reserve University, a M.S.M.E. degree from the University of Toledo, and a B.S.M.E. from Cleveland State University. He has authored/co-authored 119 technical publications to date in the drive system area, and has been the Government manager for 37 contractor reports. He is also a Fellow of the American Society of Mechanical Engineers, previous Associate Technical Editor for power transmission and gearing for the Journal of Mechanical Design, and past Chairman of the ASME Power Transmission and Gearing Committee.